Magnetization reversal in epitaxial exchange-biased IrMn/FeGa bilayers with anisotropy geometries controlled by oblique deposition

Yao Zhang,[1,2,3] Qingfeng Zhan,[1,2,*] Zhenghu Zuo,[1,2] Huali Yang,[1,2] Xiaoshan Zhang,[1,2] Guohong Dai,[1,2] Yiwei Liu,[1,2] Ying Yu,[1,2] Jun Wang,[3] Baomin Wang,[1,2] and Run-Wei Li[1,2,†]

[1]*Key Laboratory of Magnetic Materials and Devices, Ningbo Institute of Material Technology and Engineering, Chinese Academy of Sciences, Ningbo 315201, China*

[2]*Zhejiang Province Key Laboratory of Magnetic Materials and Application Technology, Ningbo Institute of Material Technology and Engineering, Chinese Academy of Sciences, Ningbo 315201, China*

[3]*Department of Physics, Ningbo University, Ningbo 315211, China*

(Received 25 January 2015; revised manuscript received 6 April 2015; published 12 May 2015)

We fabricated epitaxial exchange biased (EB) IrMn/FeGa bilayers by oblique deposition and systematically investigated their magnetization reversal. Two different configurations with the uniaxial magnetic anisotropy K_u parallel and perpendicular to the unidirectional anisotropy K_{eb} were obtained by controlling the orientation of the incident FeGa beam during deposition. A large ratio of K_u/K_{eb} was obtained by obliquely depositing the FeGa layer to achieve a large K_u while reducing the IrMn thickness to obtain a small K_{eb}. Besides the previously reported square loops, conventional asymmetrically shaped loops, and one-sided and two-sided two-step loops, unusual asymmetrically shaped loops with a three-step magnetic transition for the descending branch and a two-step transition for the ascending branch and biased three-step loops were observed at various field orientations in the films of both IrMn ($t_{\mathrm{IrMn}} = 1.5$ to 20 nm)/FeGa (10 nm) with $K_u \perp K_{eb}$ and IrMn ($t_{\mathrm{IrMn}} \leqslant 2$ nm)/FeGa (10 nm) with $K_u || K_{eb}$. Considering the geometries of anisotropies, a model based on domain wall nucleation and propagation was employed to quantitatively describe the angular dependent behaviors of IrMn/FeGa bilayers. The biased three-step magnetic switching was predicted to take place when $|K_u| > \varepsilon_{90^\circ} + K_{eb}$, where ε_{90° is the 90° domain wall nucleation energy, and the EB leads to the appearance of the unusual asymmetrically shaped hysteresis loops.

DOI: 10.1103/PhysRevB.91.174411 PACS number(s): 75.70.Cn, 75.60.Jk, 75.30.Gw

I. INTRODUCTION

FeGa alloys exhibit great promise in actuator and sensor applications due to the moderate magnetostriction of 350 ppm under very low magnetic fields, the low hysteresis, and the high tensile strength [1,2]. Recently, with the development of magnetostrictive materials applied in multiferroic composite, spintronic, and microwave devices, FeGa alloys in thin-film form have attracted extensive attention [3–6]. In various thin-film structures, exchange bias (EB) heterostructures induced by interfacial exchange coupling between ferromagnetic (FM) and antiferromagnetic (AFM) materials have been employed to stabilize the magnetization in spintronic devices [7–9], enhance the FM resonance frequency in microwave devices [10], and induce the magnetoelectric coupling in multiferroic composite [11]. Previously, we have fabricated polycrystalline IrMn/FeGa EB heterostructures on flexible substrates [12]. The EB field, coercive field, and remanence ratio of the films could be sensitively changed by the mechanical stress. However, due to the average of crystallographic orientations and inherent stresses, polycrystalline FeGa thin films exhibit a reduced magnetostriction less than 100 ppm [13]. Parkes *et al.* [3] have epitaxially grown FeGa thin film on single-crystalline substrates and achieved magnetostriction as large as the value of the bulk counterpart. This observation suggests that single-crystalline FeGa films, when integrated into the magnetoelectric materials and devices, could significantly improve their magnetomechanical behaviors, which illustrates the importance of fabricating epitaxial FeGa/AFM EB heterostructures and controlling their magnetic properties.

Exchange bias essentially establishes a unidirectional anisotropy and an accompanied uniaxial anisotropy, which breaks the symmetry of magnetization reversal [14]. In epitaxial EB systems, the intrinsic magnetocrystalline anisotropy needs to be further taken into account. Depending on the strengths and the relative orientations, the different configurations of magnetic anisotropies would give rise to complicated magnetic switching processes. For example, square, asymmetrically shaped, biased two-step, and unbiased two-step loops have been observed in *c* axis oriented epitaxial MnPd/Fe EB bilayers when measuring at different field orientations [15]. Conventionally, the EB-induced uniaxial anisotropy is aligned along the unidirectional anisotropy. In contrast, an orthogonal configuration of uniaxial and unidirectional anisotropies has been observed in the *a* axis oriented epitaxial MnPd/Fe EB bilayers due to the spin-flop coupling in the spin compensated FM-AFM interfaces [16]. In such a system, the transverse uniaxial anisotropy intrinsically depends on the interface exchange coupling, and it therefore could not be set at the required strength and orientation. In this paper, epitaxial IrMn/FeGa EB bilayers, which are important for applications in magnetostrictive alloys in thin-film spintronics, microwave devices, and multiferroic composites, have been fabricated on single-crystalline MgO(001) substrates. The oblique deposition was used to set a uniaxial anisotropy parallel or perpendicular to the EB. The strength of unidirectional anisotropy was changed by varying the thickness of the AFM layer. Three-step loops with EB and an unusual asymmetrically

*zhanqf@nimte.ac.cn
†runweili@nimte.ac.cn

shaped loop with three-step magnetic transition for the descending branch and two-step transition for the ascending branch were obtained in the IrMn/FeGa heterostructures with well-defined geometries of magnetic anisotropies. A phenomenological model based on the domain wall (DW) nucleation and propagation was employed to quantitatively describe the occurrence of magnetic switching processes in the epitaxial EB system at various field orientations.

II. EXPERIMENT

$Ir_{20}Mn_{80}$ (t_{IrMn})/$Fe_{81}Ga_{19}$ (10 nm) bilayers were epitaxially deposited on optically transparent single-crystalline MgO(001) substrates in a magnetron sputtering system with a base pressure below 3×10^{-7} torr. The substrates were annealed at 700 °C for 1 h in a vacuum chamber and then held at 250 °C during deposition. FeGa layers were obliquely deposited at an incidence angle of 45°. The projection of FeGa atom flux on the plane of the substrates was set parallel or perpendicular to the MgO[110] direction, i.e., the FeGa[010] direction. This geometry of oblique deposition has been demonstrated to introduce a strong uniaxial anisotropy perpendicular to the projection of the magnetic atom flux and remarkably change the magnetization reversal of epitaxial magnetic films [17]. The IrMn layers were deposited while continuously rotating the substrates. A reference IrMn/FeGa sample was fabricated with the deposition angle of 45° but rotating the substrate during the growth of both FeGa and IrMn layers. In order to induce an EB along the FeGa[010] direction, a magnetic field of 500 Oe provided by a permanent magnet was applied along the MgO[110] axis during growth. After deposition, a 3 nm protective Ta layer was deposited on the samples to avoid oxidation.

The crystalline structure of IrMn/FeGa heterostructures was characterized by x-ray diffraction (XRD) with Cu $K\alpha$ radiation using a Rigaku D/Max-2500. In the θ-2θ XRD pattern [Fig. 1(a)], the (002) peaks of FeGa and IrMn indicate a good (002) out-of-plane texture. Furthermore, the x-ray in-plane Φ scans [Fig. 1(b)] display a fourfold symmetry and confirm the epitaxial relationship of MgO(001)[100] ∥ FeGa(001)[110]. The surface morphology was characterized by atomic force microscopy using a Veeco Dimension 3100V. The atomic force microscopy image confirms a smooth surface morphology of the epitaxial EB films with a root-mean-square roughness of 0.9 nm [Fig. 1(c)]. The longitudinal (∥) and transverse (⊥) magneto-optical Kerr effect (MOKE) measurements were used to study the magnetic switching processes of epitaxial IrMn/FeGa bilayers by illuminating the samples from the bottom side through the transparent MgO(001) substrates.

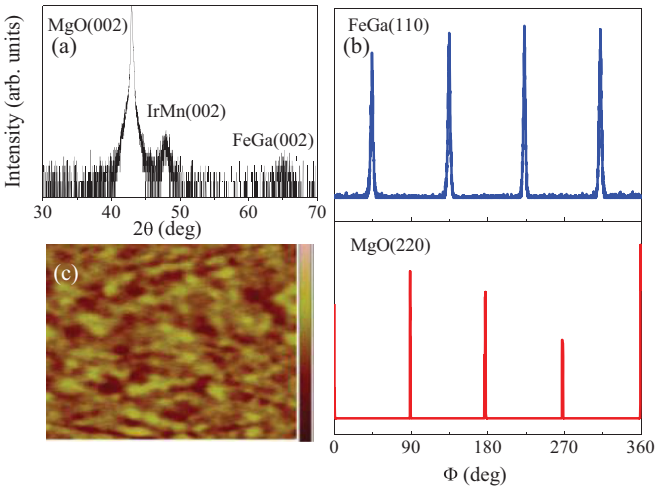

FIG. 1. (Color online) X-ray diffraction measurements (a) θ-2θ scan and (b) in-plane Φ scans, for the rotational sample of IrMn (20 nm)/FeGa (10 nm) with $K_u||K_{eb}$. (c) Atomic force microscopy image ($2 \times 2\,\mu m^2$) of the IrMn (20 nm)/FeGa (10 nm) film with $K_u||K_{eb}$ grown by oblique deposition. The color contrast (dark to bright) for the height scale corresponds to 10 nm.

III. EXPERIMENTAL RESULTS AND DISCUSSION

The anisotropy geometries and the magnetic switching routes defined in this paper are summarized in Fig. 2. The EB gives rise to a unidirectional anisotropy K_{eb} and a collinear uniaxial anisotropy along the field-cooling direction. Additionally, the oblique deposition of the FeGa layer induces an additional uniaxial anisotropy parallel or perpendicular to the EB. The two collinear or orthogonal uniaxial anisotropies, depending on their relative strengths and orientations, are essentially equivalent to a single uniaxial anisotropy K_u with the orientation parallel or perpendicular to the EB. These anisotropies are superimposed on the intrinsic FeGa fourfold magnetocrystalline anisotropy K_1, which therefore induces various magnetic switching routes between the FeGa easy axes when the external magnetic field H is applied along different orientations. According to the initial and the final remnant directions involved in the magnetic transitions, we define the corresponding 90° magnetic switching fields as H_{c1} to H_{c4} in clockwise direction and H_{cI} to H_{cIV} in counterclockwise direction, respectively. The switching fields for 180° magnetic switching from FeGa[0$\bar{1}$0] to FeGa[010] and from FeGa[010] to FeGa[0$\bar{1}$0] are H_c and $H_{c'}$, respectively. It is noted that

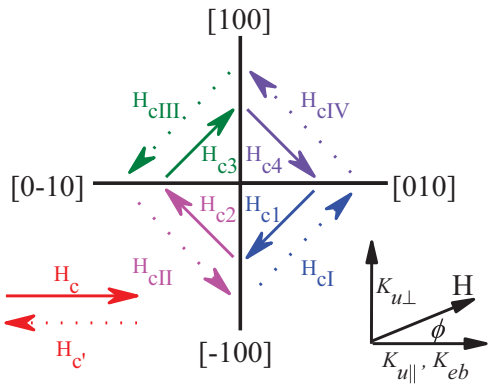

FIG. 2. (Color online) The geometries of anisotropies for the epitaxial IrMn/FeGa EB bilayers. A uniaxial anisotropy along or perpendicular to the FeGa[010] axis induced by oblique deposition and the EB induced unidirectional anisotropy along the FeGa[010] axis are superimposed on the FeGa cubic anisotropy. The coercive fields for the magnetic switching between different FeGa easy axes are defined. The external field is applied at an angle of ϕ with respect to the EB.

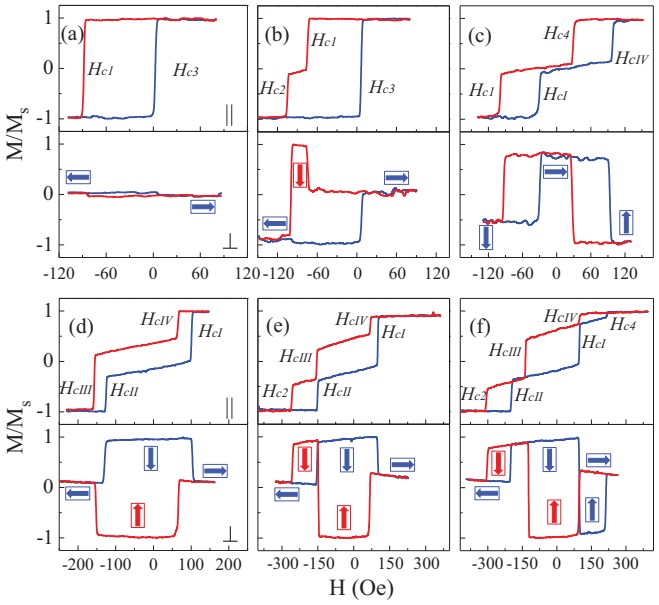

FIG. 3. (Color online) Typical longitudinal (∥) and transverse (⊥) MOKE loops measured at various field orientations. (a) Square loop, (b) asymmetrically shaped loop, and (c) one-side two-step loop are obtained at $\phi = 0°$, 20°, and 90°, respectively, for the reference IrMn (20 nm)/FeGa (10 nm) bilayer with $K_u||K_{eb}$. (d) Two-side two-step loop, (e) unusual asymmetrically shaped loop, and (f) biased three-step loop are obtained at $\phi = 5°$, 20°, and 25°, respectively, for the IrMn (20 nm)/FeGa (10 nm) bilayer with $K_u \perp K_{eb}$. The red and blue curves correspond to the descending and ascending branches of the hysteresis loops, respectively. The arrows enclosed by a square represent the orientation of FeGa spins. The coercive fields based on the magnetic switching routes are presented as well.

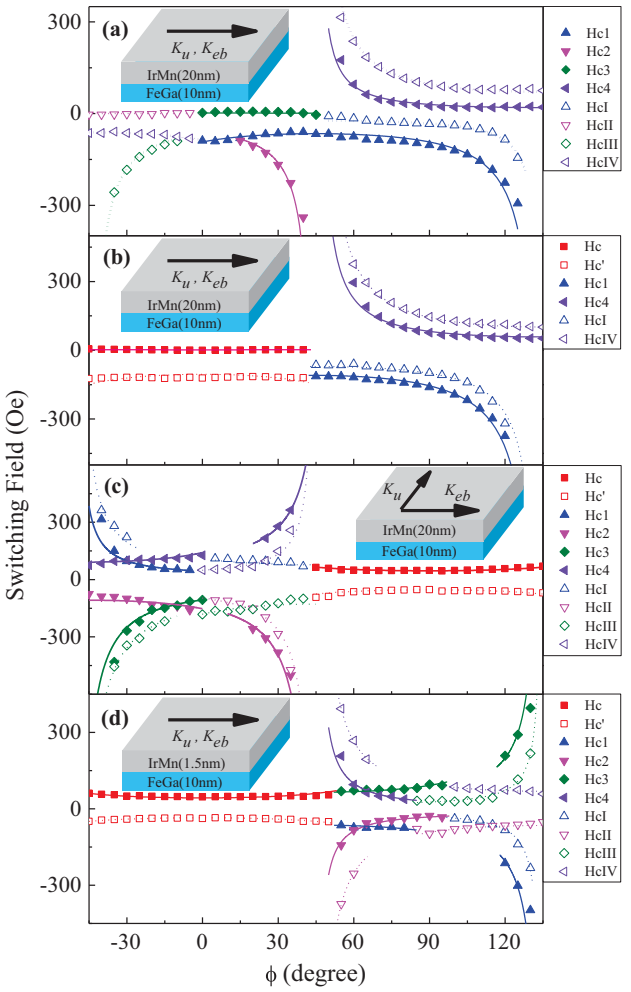

FIG. 4. (Color online) Typical field orientation dependence of the experimentally observed switching fields (symbols) and the corresponding theoretical fitting results (curves) for (a) the reference IrMn (20 nm)/FeGa (10 nm) bilayer with $K_u||K_{eb}$ grown by rotating substrates, the obliquely deposited films of (b) IrMn (20 nm)/FeGa (10 nm) with $K_u||K_{eb}$, (c) IrMn (20 nm)/FeGa (10 nm) with $K_u \perp K_{eb}$, and (d) IrMn (1.5 nm)/FeGa (10 nm) with $K_u||K_{eb}$.

the crystalline directions used in this paper refer to the FeGa lattice, unless indicated otherwise.

Both longitudinal and transverse hysteresis loops are obtained at different external field orientations ϕ in an interval of 5°. For the reference sample of an IrMn (20 nm)/FeGa (10 nm) bilayer fabricated with rotating substrate during the growth of both IrMn and FeGa, the square loops shifted to the negative direction are observed for ϕ around the EB direction, and the corresponding transverse MOKE signal indicates the magnetization switches between the [010] and [0$\bar{1}$0] axes via DW nucleation and propagation [Fig. 3(a)]. Conventional asymmetrically shaped loops with two-step magnetic transitions for the descending branch but a one-step magnetic transition for the ascending branch are observed at $\phi = 20°$, and the orientation of FeGa spins in the magnetic switching process can be obtained from the corresponding transverse MOKE signal [Fig. 3(b)]. Close to the perpendicular of EB, that is, $45° < \phi < 135°$, we observe one-side two-step loops in which the magnetic switching routes for both branches are mediated via the same FeGa easy axes determined by the EB [Fig. 3(c)]. In the case of decreasing the thicknesses of the AFM layer to reduce K_{eb}, the one-side two-step loops will be gradually replaced by the two-side two-step loops in which the magnetization reversals for descending and ascending branches are mediated via the opposite FeGa easy axes. The angular dependence of switching fields for the reference sample shows a clear asymmetry about $\phi = 90°$ [Fig. 4(a)], indicating the broken symmetry of magnetic anisotropies about $\phi = 90°$ by K_{eb}. The critical angle ϕ_1 separating the occurrence of the square and conventional asymmetrically shaped loops is around 15°.

It is well known that K_u could be produced not only by the EB but also by oblique deposition. A number of researchers have employed oblique deposition to tune both the strength and the orientation of K_u, and thus control the magnetic switching processes [17–20]. For example, three-step magnetic transitions have been obtained in epitaxial Fe/MgO(001) films by using oblique deposition to introduce a K_u superimposed on the cubic anisotropy of Fe [17]. In an epitaxial EB system, if the strength and orientation of K_u can be changed by oblique deposition, the multistep magnetic switching processes could be well controlled. In order to investigate the effect of K_u on the magnetic reversal in epitaxial EB bilayers, we fabricated the IrMn (20 nm)/FeGa (10 nm)

films by obliquely depositing the FeGa layer perpendicular and parallel to the EB, which respectively results in K_u parallel and perpendicular to the EB. For the sample with $K_u||K_{eb}$, the magnetic measurements indicate that the one-side two-step magnetic switching event occurs in the range of $45° < \phi < 135°$, which is similar to the reference sample grown by rotating substrates. However, when $-45° < \phi < 45°$, only the square loops with EB can be observed. The corresponding angular dependence of the magnetic switching fields is shown in Fig. 4(b). The angular dependent behaviors indicate that the enhanced K_u produced by the oblique deposition favors the occurrence of the one-step loops and constrains the appearance of the conventional asymmetrically shaped loops with a one-step branch and a two-step opposite branch, that is, increasing the critical angle ϕ_1 separating the two types of magnetic switching.

For the IrMn (20 nm)/FeGa (10 nm) film with $K_u \perp K_{eb}$, the hysteresis loop measured at $\phi = 0°$ exhibits a feature of one-side two-step magnetic switching. For $\phi = 5°$, the two-side two-step loop is observed with the intermediate axes of [100] for the descending branch and $[\bar{1}00]$ for the ascending branch [Fig. 3(d)]. For $\phi = 20°$, an unusual asymmetrically shaped loop is observed with three-step magnetic switching of $[010] \rightarrow [100] \rightarrow [\bar{1}00] \rightarrow [0\bar{1}0]$ occurring at the descending branch and two-step magnetic switching of $[0\bar{1}0] \rightarrow [\bar{1}00] \rightarrow [010]$ showing at the ascending branch [Fig. 3(e)]. With further rotation of the magnetic field to 25°, the ascending branch changes to three-step magnetic switching with a route of $[0\bar{1}0] \rightarrow [\bar{1}00] \rightarrow [100] \rightarrow [010]$; thus, the hysteresis loop displays a feature of three-step magnetic switching with a shift induced by the EB [Fig. 3(f)]. The ϕ dependence of switching fields for the IrMn (20 nm)/FeGa (10 nm) film with $K_u \perp K_{eb}$ is summarized in Fig. 4(c). The critical angles ϕ_2, ϕ_3, and ϕ_4 separating the occurrence of the one-side two-step loops, the two-side two-step loops, the unusual asymmetrically shaped loops, and the biased three-step loops are about 5°, 20°, and 25°, respectively.

The EB induced unidirectional anisotropy K_{eb} is another key factor in determining the magnetic switching of EB bilayers. The previously studied epitaxial systems usually possess comparable K_{eb} and K_u. Changing the EB will lead to a corresponding variation of K_u [15,21]. In an experiment, a large ratio of K_u/K_{eb} can be well defined by obliquely depositing a FM layer to achieve a large K_u while reducing the AFM thickness to obtain a small K_{eb}, which could significantly change the magnetic switching. In order to obtain a large K_u/K_{eb} in the EB system, we fabricated the samples of IrMn/FeGa (10 nm) with the t_{IrMn} less than 20 nm and oblique deposition of the FeGa layer. When $t_{\mathrm{IrMn}} \leqslant 2$ nm, the films with $K_u||K_{eb}$ display the distinct angular dependent behaviors. For instance, the IrMn (1.5 nm)/FeGa (10 nm) bilayer exhibits the biased square loops, the biased three-step loops, the unusual asymmetrically shaped loops, the two-side two-step loops, and the one-side two-step loops in $-45° < \phi < 45°$, $55° < \phi < 60°$, $60° < \phi < 65°$, $65° < \phi < 80°$, and $80° < \phi < 90°$, respectively. The corresponding angular dependence of the magnetic switching fields is shown in Fig. 4(d). In contrast, the IrMn($t_{\mathrm{IrMn}} < 20$ nm)/FeGa (10 nm) films with a thin IrMn layer and $K_u \perp K_{eb}$ display similar features of magnetic reversal as the IrMn (20 nm)/FeGa (10 nm) sample with $K_u \perp K_{eb}$, and therefore they are not shown here.

IV. MAGNETIZATION REVERSAL MECHANISM

In order to understand the role of K_u and K_{eb} in determining the unusual magnetization reversal processes, a model based on DW nucleation and propagation is employed to describe the angular dependent behaviors of IrMn/FeGa EB bilayers with different geometries of anisotropies. The total free energy contains the intrinsic cubic magnetocrystalline term, the uniaxial magnetic anisotropy term, the unidirectional magnetic anisotropy term, and the Zeeman energy, and it can be written as

$$E = (K_1/4)\sin^2 2\theta - K_u \cos^2\theta - K_{eb}\cos\theta - MH\cos(\phi - \theta),$$

where M is the saturation magnetization, H is the external magnetic field, and θ is the angle between M and H. The sign of K_u represents the orientation of K_u, that is, positive for $K_u||K_{eb}$ and negative for $K_u \perp K_{eb}$.

The switching fields can be achieved by the energy gain between the local minima at the initial and final easy axes involved in the magnetic transition [22]. The theoretical switching fields for the 90° magnetic transitions can be obtained as

$$H_{c1} = \frac{\varepsilon_{90°} + K_{eb} + K_u}{M(-\sin\phi - \cos\phi)}, \quad H_{c2} = \frac{\varepsilon_{90°} + K_{eb} - K_u}{M(\sin\phi - \cos\phi)},$$

$$H_{c3} = \frac{\varepsilon_{90°} - K_{eb} + K_u}{M(\sin\phi + \cos\phi)}, \quad H_{c4} = \frac{\varepsilon_{90°} - K_{eb} - K_u}{M(-\sin\phi + \cos\phi)},$$

$$H_{c\mathrm{I}} = \frac{\varepsilon_{90°} - K_{eb} - K_u}{M(\sin\phi + \cos\phi)}, \quad H_{c\mathrm{II}} = \frac{\varepsilon_{90°} - K_{eb} + K_u}{M(-\sin\phi + \cos\phi)},$$

$$H_{c\mathrm{III}} = \frac{\varepsilon_{90°} + K_{eb} - K_u}{M(-\sin\phi - \cos\phi)}, \quad H_{c\mathrm{IV}} = \frac{\varepsilon_{90°} + K_{eb} + K_u}{M(\sin\phi - \cos\phi)},$$

where $\varepsilon_{90°}$ is the 90° DW nucleation energy.

For the 180° magnetic switching from $[0\bar{1}0]$ to [010],

$$H_c = \frac{\varepsilon_{180°} - 2K_{eb}}{2M\cos\phi},$$

and for the inverse magnetic switching from [010] to $[0\bar{1}0]$,

$$H_{c'} = -\frac{\varepsilon_{180°} + 2K_{eb}}{2M\cos\phi},$$

where $\varepsilon_{180°}$ is the 180° DW nucleation energy. The detailed derivation for these equations can be seen elsewhere [15].

In previous papers on epitaxial Fe films with a weak K_u, we found that the 90° magnetic switching processes could be interpreted by the 90° DW nucleation. In contrast, the 180° magnetic switching processes in both the square and three-step loops could be well described by a model of two successive 90° DW nucleations, but not the 180° DW nucleation [23,24]. In a subsequent paper on epitaxial MnPd/Fe EB bilayers with a rather strong K_{eb} and K_u [15], the 180° magnetic switching behavior in the square loop changed to the 180° DW nucleation. In the present IrMn/FeGa EB heterostructures, the angular dependence of 90° magnetic switching fields can be easily explained by the corresponding theoretical equations based on the 90° DW nucleation [Figs. 4(a) to 4(d)]. On the other hand, the 180° magnetic switching appears in the

square loops, the conventional asymmetrically shaped loops, the unusual asymmetrically shaped loops, and the biased three-step loops. The switching fields for the 180° magnetic transitions between $[0\bar{1}0]$ and [010] occurring in the reference sample of IrMn (20 nm)/FeGa (10 nm) with $K_u||K_{eb}$ [see both branches of the square loop in Fig. 3(a) and the ascending branch of the conventional asymmetrically shaped loop in Fig. 3(b)] can be nicely fitted by the equations for H_{c3} and H_{c1}, but not the equations for H_c or $H_{c'}$, which suggests that these 180° magnetic transitions are mediated via the intermediate axes of [100] or $[\bar{1}00]$ following the reversal mechanism of two successive 90° DW nucleations [Fig. 4(a)]. For the IrMn (20 nm)/FeGa (10 nm) film with $K_u\perp K_{eb}$, the 180° magnetic switching between [100] and $[\bar{1}00]$ occurring in the descending branch of the unusual asymmetrically shaped loops [see Fig. 3(e)] and both branches of the biased three-step loops [see Fig. 3(f)] can also be described with the model of two successive 90° DW nucleations [Fig. 4(c)]. In contrast, the switching fields for the square loops obtained in the obliquely deposited IrMn/FeGa films with different geometries of anisotropies and various IrMn thickness need to be fitted by the equations for H_c and $H_{c'}$ based on the 180° DW nucleation [Figs. 4(b) to 4(d)].

The critical angles separating the appearance of different magnetic switching routes can be predicted by comparing the switching fields given by different possible routes. For the reference sample of IrMn (20 nm)/FeGa (10 nm) with $K_u||K_{eb}$, the magnetic switching processes in the range of $0° < \phi < 45°$ are determined by the comparison between H_{c1} and H_{c2}. The relations of $H_{c1} > H_{c2}$ and $H_{c1} < H_{c2}$ correspond to the occurrence of two successive and two separate 90° DW nucleations in the descending branch, respectively. Consequently, one can obtain the critical angle $\phi_1 = \arctan[K_u/(\varepsilon_{90°} + K_{eb})]$, which separates the square and conventional asymmetrically shaped loops. For the obliquely deposited IrMn (t_{IrMn} = 1.5 to 20 nm)/FeGa (10 nm) films with $K_u\perp K_{eb}$, in the range of $0° < \phi < 45°$, the two-side two-step magnetic switching can be induced in the descending branch when $H_{cIII} > H_{cII}$, and the three-step magnetic switching occurs in the descending branch when $H_{cIII} < H_{cII}$ [see Figs. 3(d) and 3(e)]. On the other hand, the relation of $H_{cI} > H_{cIV}$ leads to the two-step magnetic transition in the ascending branch. Thus, the critical angle $\phi_3 = \arctan[\varepsilon_{90°}/(|K_u| + K_{eb})]$ separating the two-side two-step loops and the unusual asymmetrically shaped loops can be obtained. With a further increase in ϕ, in the case of both $H_{cI} < H_{cIV}$ and $H_{cIII} < H_{cII}$, the biased three-step switching route can be observed [see Fig. 3(f)]. As a result, the critical angle $\phi_4 = \arctan[\varepsilon_{90°}/(|K_u| - K_{eb})]$ separating the unusual asymmetrically shaped loops and the biased three-step loops can be obtained. It should be noted that we have experimentally observed the one-side two-step loops at $\phi = 0°$ in this kind of sample with $K_u\perp K_{eb}$. However, the energy barrier of $\Delta E_{[010]\to[100]}$ in this scenario is equal to $\Delta E_{[010]\to[\bar{1}00]}$, and so the probabilities for the magnetic switching mediated through the [100] or $[\bar{1}00]$ axes are identical. Consequently, we cannot in theory obtain the critical angle ϕ_2, which separates the one-side two-step and two-side two-step loops. We ascribe the observation of the one-side two-step loops to the imperfect configuration of $K_u\perp K_{eb}$ due to the experimental limitation. For the IrMn (1.5 nm)/FeGa (10 nm) sample with $K_u||K_{eb}$, the one-side two-step and the two-side two-step magnetic switching routes take place when the relations of $H_{cIII} > H_{c4}$ and $H_{cIII} < H_{c4}$ are respectively satisfied in the range of $45° < \phi < 90°$. As a result, the critical angle $\phi_2' = \arctan[(\varepsilon_{90°} - K_u)/K_{eb}]$ is obtained. In addition, according to the comparisons between H_{c3} and H_{c4} and between H_{c1} and H_{c2}, one can obtain the critical angles $\phi_3' = \arctan[K_u/(\varepsilon_{90°} - K_{eb})]$ and $\phi_4' = \arctan[K_u/(\varepsilon_{90°} + K_{eb})]$, which respectively separate the two-side two-step loops, the unusual asymmetrically shaped loops, and the biased three-step loops in the range of $45° < \phi < 90°$. Both expressions of ϕ_4 for $K_u\perp K_{eb}$ and ϕ_4' for $K_u||K_{eb}$ indicate that the biased three-step magnetic switching takes place when $|K_u| > \varepsilon_{90°} + K_{eb}$. The EB, i.e., $K_{eb} > 0$, ensures the differences between ϕ_3 and ϕ_4 and between ϕ_3' and ϕ_4', which lead to the appearance of the unusual asymmetrically shaped hysteresis loops.

Using the model based on the DW nucleation, the angular dependence of switching fields for IrMn/FeGa epitaxial EB bilayers with various geometries of anisotropies can be nicely fitted [Figs. 4(a) to 4(d)]. For the reference sample of IrMn (20 nm)/FeGa (10 nm) with $K_u||K_{eb}$, the fitting for the experimental data gives the parameters $\varepsilon_{90°}/M = 39.8$ Oe, $K_u/M = 14.0$ Oe, and $K_{eb}/M = 50.4$ Oe. As a result, the critical angle ϕ_1 separating the square loops and the conventional asymmetrically shaped loops can be predicted at 8.8°. For the obliquely deposited IrMn (1.5 nm)/FeGa (10 nm) film with $K_u||K_{eb}$, the fitting parameters are $\varepsilon_{90°}/M = 31.0$ Oe, $K_u/M = 63.8$ Oe, and $K_{eb}/M = 3.1$ Oe. One can theoretically predict that the biased three-step loops, the unusual asymmetrically shaped loops, the two-side two-step loops, and the one-side two-step loops take place in $45° < \phi < 61.9°$, $61.9° < \phi < 66.4°$, $66.4° < \phi < 84.6°$, and $84.6° < \phi < 90°$, respectively. For the obliquely deposited IrMn (20 nm)/FeGa (10 nm) with $K_u||K_{eb}$, we obtain the fitting parameters as $\varepsilon_{90°}/M = 46.5$ Oe, $K_u/M = 73.0$ Oe, and $K_{eb}/M = 44.6$ Oe. In case of $K_u\perp K_{eb}$, the obliquely deposited IrMn (20 nm)/FeGa (10 nm) sample, using the fitting parameters $\varepsilon_{90°}/M = 46.1$ Oe, $K_u/M = -107.4$ Oe, and $K_{eb}/M = 25.1$ Oe, one can theoretically predict that the unusual asymmetrically shaped loops and the biased three-step loops appear in the range of $19.2° < \phi < 29.3°$ and $29.3° < \phi < 45°$, respectively. The theoretically predicted range of ϕ in which the different magnetic switching processes occur agrees well with the experimental observations. According to the criterion for the occurrence of the biased three-step magnetic switching and the unusual asymmetrically magnetic switching, that is, $|K_u| > \varepsilon_{90°} + K_{eb}$, one can understand why these special loops appear in the obliquely deposited IrMn (1.5 nm)/FeGa (10 nm) film with $K_u||K_{eb}$ and IrMn (t_{IrMn} = 1.5 to 20 nm)/FeGa (10 nm) films with $K_u\perp K_{eb}$, but not the obliquely deposited IrMn (20 nm)/FeGa (10 nm) sample with $K_u||K_{eb}$.

The obliquely deposited IrMn (20 nm)/FeGa (10 nm) films with $K_u||K_{eb}$ or $K_u\perp K_{eb}$ have similar $\varepsilon_{90°}$, which is larger than that for the reference sample and IrMn (1.5 nm)/FeGa (10 nm) with $K_u||K_{eb}$. The different values of $\varepsilon_{90°}$ can be understood by considering the interfacial roughness and the rotatable AFM spins at the FM/AFM interface. The oblique deposition can increase the interfacial roughness to act as the pinning centers

for DW nucleation and therefore enhance the value of ε_{90° [17]. However, the rotatable Mn spins near the interface, which are strongly coupled with FeGa moments and may follow the motion of the FeGa layer, can also result in an increase of ε_{90° [25]. For the films with the identically bilayered structure of IrMn (20 nm)/FeGa (10 nm), the reference sample grown with rotating substrate displays the largest K_{eb}. Moreover, the value of K_{eb} for the obliquely deposited sample with $K_u \perp K_{eb}$ is much smaller than that for the sample with $K_u || K_{eb}$. The oblique deposition plays an important role in the value of K_{eb}. The rough interface caused by the oblique deposition induces the different orientations of AFM spins, and thus the total number of AFM spins pinning the FM moments in one direction is reduced, concurrently reducing the strength of K_{eb} [26]. In addition, different from the sample with $K_u || K_{eb}$, the FM and AFM spins in the obliquely deposited sample with $K_u \perp K_{eb}$ are preferentially aligned perpendicular to each other, which leads to the significant reduction of interfacial exchange coupling between them.

In conclusion, we have prepared IrMn/FeGa EB epitaxial bilayers on MgO(001) substrates by oblique deposition at an incidence angle of 45°, which can induce a large K_u in the FeGa layer. Two different configurations of anisotropies, $K_u || K_{eb}$ and $K_u \perp K_{eb}$, can be obtained by controlling the orientation of the incident FeGa beam during deposition. By reducing t_{IrMn} as well as K_{eb}, a large ratio of K_u/K_{eb} can be obtained. The square loops, the conventional asymmetrically shaped loops, and the one-side two-step loops were observed at various field orientations in the rotational reference sample of IrMn (20 nm)/FeGa (10 nm) with $K_u || K_{eb}$. Besides these loops, the two-side two-step loops, the unusual asymmetrically shaped loops, and the biased three-step loops were observed in the films of IrMn ($t_{\mathrm{IrMn}} = 1.5$ to 20 nm)/FeGa (10 nm) with $K_u \perp K_{eb}$ and IrMn ($t_{\mathrm{IrMn}} \leqslant 2$ nm)/FeGa (10 nm) with $K_u || K_{eb}$. Considering the anisotropies of FeGa films, a model based on DW nucleation and propagation was employed to quantitatively describe the angular dependent switching fields of IrMn/FeGa epitaxial bilayers and predict the range of ϕ where the different magnetic switching processes occur. The condition for the appearance of the biased three-step loops in epitaxial EB systems was established, that is, $|K_u| > \varepsilon_{90^\circ} + K_{eb}$. Moreover, the EB leads to the occurrence of the unusual asymmetrically shaped hysteresis loops.

ACKNOWLEDGMENTS

The authors acknowledge the financial support from the National Natural Science Foundation of China (Grants No. 11174302 and No. 11374312).

[1] A. E. Clark, J. B. Restorff, M. Wun-Fogle, T. A. Lograsso, and D. L. Schlagel, IEEE Trans. Magn. **36**, 3238 (2000).
[2] J. Atulasimha and A. B. Flatau, Smart Mater. Struct. **20**, 043001 (2011).
[3] D. E. Parkes, L. R. Shelford, P. Wadley, V. Holý, M. Wang, A. T. Hindmarch, G. van der Laan, R. P. Campion, K. W. Edmonds, S. A. Cavill, and A. W. Rushforth, Sci. Rep. **3**, 2220 (2013).
[4] B. K. Kuanr, R. E. Camley, Z. Celinski, A. McClure, and Y. Idzerda, J. Appl. Phys. **115**, 17C112 (2014).
[5] J. Lou, M. Liu, D. Reed, Y. Ren, and N. X. Sun, Adv. Mater. **21**, 4711 (2009).
[6] Y. L. Xie, Q. F. Zhan, Y. W. Liu, G. H. Dai, H. L. Yang, Z. H. Zuo, B. Chen, B. M. Wang, Y. Zhang, X. Rong, and R.-W. Li, AIP Adv. **4**, 117113 (2014).
[7] W. H. Meiklejohn and C. P. Bean, Phys. Rev. **102**, 1413 (1956).
[8] C. Chappert, A. Fert, and F. N. Van Dau, Nat. Mater. **6**, 813 (2007).
[9] S. A. Wolf, D. D. Awschalom, R. A. Buhrman, J. M. Daughton, S. von Molnar, M. L. Roukes, A. Y. Chtchelkanova, and D. M. Treger, Science **294**, 1488 (2001).
[10] N. N. Phuoc, F. Xu, and C. K. Ong, Appl. Phys. Lett. **94**, 092505 (2009).
[11] Y. H. Chu, L. W. Martin, M. B. Holcomb, M. Gajek, S. J. Han, Q. He, N. Balke, C. H. Yang, D. Lee, W. Hu, Q. Zhan, P. L. Yang, A. Fraile-Rodriguez, A. Scholl, S. X. Wang, and R. Ramesh, Nat. Mater. **7**, 478 (2008).
[12] X. S. Zhang, Q. F. Zhan, G. H. Dai, Y. W. Liu, Z. H. Zuo, H. L. Yang, B. Chen, and R.-W. Li, Appl. Phys. Lett. **102**, 022412 (2013).
[13] J. L. Dean, M. T. Bryan, N. A. Morley, G. Hrkac, A. Javed, M. R. J. Gibbs, and D. A. Allwood, J. Appl. Phys. **110**, 043902 (2011).
[14] S. Brems, K. Temst, and C. Van Haesendonck, Phys. Rev. Lett. **99**, 067201 (2007).
[15] Q. F. Zhan, W. Zhang, and K. M. Krishnan, Phys. Rev. B **83**, 094404 (2011).
[16] Q. F. Zhan and K. M. Krishnan, Appl. Phys. Lett. **96**, 112506 (2010).
[17] Q. F. Zhan, C. Van Haesendonck, S. Vandezande, and K. Temst, Appl. Phys. Lett. **94**, 042504 (2009).
[18] S. van Dijken, G. DiSanto, and B. Poelsema, Phys. Rev. B **63**, 104431 (2001).
[19] S. Cherifi, R. Hertel, A. Locatelli, Y. Watanabe, G. Potdevin, A. Ballestrazzi, M. Balboni, and S. Heun, Appl. Phys. Lett. **91**, 092502 (2007).
[20] Y. P. Fang, W. He, H. L. Liu, Q. F. Zhan, H. F. Du, Q. Wu, H. T. Yang, X. Q. Zhang, and Z. H. Cheng, Appl. Phys. Lett. **97**, 022507 (2010).
[21] W. Zhang, M. E. Bowden, and K. M. Krishnan, Appl. Phys. Lett. **98**, 092503 (2011).
[22] R. P. Cowburn, S. J. Gray, and J. A. C. Bland, Phys. Rev. Lett. **79**, 4018 (1997).
[23] Q. F. Zhan, S. Vandezande, K. Temst, and C. Van Haesendonck, Phys. Rev. B **80**, 094416 (2009).
[24] Q. F. Zhan, S. Vandezande, K. Temst, and C. Van Haesendonck, New J. Phys. **11**, 063003 (2009).
[25] S. Brück, G. Schütz, E. Goering, X. Ji, and K. M. Krishnan, Phys. Rev. Lett. **101**, 126402 (2008).
[26] J. Nogués, T. J. Moran, D. Lederman, I. K. Schuller, and K. V. Rao, Phys. Rev. B **59**, 6984 (1999).